A multi-model ensemble to investigate uncertainty in the estimation of wave-driven longshore sediment transport patterns along a non-straight coastline

Zarifsanayei, Amin Reza; Antolínez, José A.A.; Etemad-Shahidi, Amir; Cartwright, Nick; Strauss, Darrell

DOI
10.1016/j.coastaleng.2022.104080

Publication date
2022

Document Version
Final published version

Published in
Coastal Engineering

Citation (APA)
Zarifsanayei, A. R., Antolínez, J. A. A., Etemad-Shahidi, A., Cartwright, N., & Strauss, D. (2022). A multi-model ensemble to investigate uncertainty in the estimation of wave-driven longshore sediment transport patterns along a non-straight coastline. *Coastal Engineering*, *173*, Article 104080. https://doi.org/10.1016/j.coastaleng.2022.104080

Coastal Engineering 173 (2022) 104080

Contents lists available at ScienceDirect

Coastal Engineering

journal homepage: www.elsevier.com/locate/coastaleng

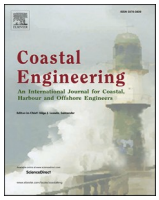

A multi-model ensemble to investigate uncertainty in the estimation of wave-driven longshore sediment transport patterns along a non-straight coastline

Amin Reza Zarifsanayei [a,c,*], José A.A. Antolínez [b], Amir Etemad-Shahidi [a,c,d], Nick Cartwright [a,c], Darrell Strauss [a,c]

[a] School of Engineering and Built Environment, Griffith University, QLD, 4222, Australia
[b] Department of Hydraulic Engineering, Faculty of Civil Engineering and Geosciences, Delft University of Technology, the Netherlands
[c] Coastal and Marine Research Centre (CMRC), Griffith University, QLD, 4222, Australia
[d] School of Engineering, Edith Cowan University, WA, 6027, Australia

ARTICLE INFO

Keywords:
Longshore sediment transport
Uncertainty ranking
Ensemble modeling
Wave transformation uncertainty

ABSTRACT

Although there have been many efforts in the literature to hindcast the patterns of longshore sediment transport (LST), they mainly disregarded uncertainty issues. Forcing datasets, wave transformation methods, and LST models are among the main sources of uncertainty in LST estimations. The combination of the aforementioned sources of uncertainty makes the estimation of LST patterns challenging for non-straight coastlines as the uncertainty ranges might vary from site to site. In this paper, a simple ensemble modeling framework was employed to investigate LST rate uncertainty at seven sites along a non-straight coastline (Gold Coast, Australia). The ensemble was formed by two different forcing datasets (i.e., integral parameters of total wave energy from two hindcast datasets of ERA5 and CAWCR), two different wave transformation methods (i.e., inclusion and exclusion of local wind effects), and eight LST models (i.e., bulk formulae and process-based models). Moreover, the relative importance of each source of uncertainty was ranked using the ANOVA-variance-based model. Finally, the weighted ensemble mean was used to investigate intra- and inter-annual variability of LST rates. The results showed that the range of uncertainty of LST rates for open coasts of Gold Coast is much higher than that of semi-sheltered coasts. On annual scale, for open coasts, 40% to 50% of total uncertainty was due to the choice of wave transformation methods, while for semi-sheltered coasts, it was 20%–30%. Moreover, almost for all sites, 30% to 50% of total uncertainty was controlled by the choice of LST models and the interaction of wave transformation methods and LST models. Although the weighted ensemble mean could provide an estimate of LST patterns along the coast, addressing the residual uncertainties (arising from other sources, discussed at the end of this paper), in future works, would help increase the certainty of the estimations.

1. Introduction

Coastal systems such as sandy coasts evolve under different coastal processes acting in different temporal and spatial scales (Masselink and Hughes, 2003). On the decadal time-scales, gradients in wave-driven longshore sediment transport (LST) and sea-level rise (SLR)-induced erosion are the key processes contributing to long-term coastal evolution (Hallin et al., 2019). While SLR-driven erosion tends to be approximately uniform along uninterrupted coastlines, LST-driven erosion/accretion varies along the coasts due to the variability of nearshore wave patterns (Antolínez et al., 2018). Given the wave forcing as the main driver of coastal sediment transport in coastal areas, understanding variations in wave patterns (e.g., wave height and direction, severity and number of storms) and the time scale of these changes is crucial to cover both short-term (e.g., 5–10 years) and long-term (e.g., 30–50 years) horizons of coastal planning.

Although hindcasting long-term patterns and magnitude of LST can provide valuable information for shoreline management plans (Mangor et al., 2017), reliable estimation of LST is still a challenging task. In this regard, different types of uncertainty need to be considered and

* Corresponding author. School of Engineering and Built Environment and Coastal & Marine Research Centre, Griffith University, Southport, QLD, 4222, Australia.
E-mail address: aminreza.zarifsanayei@griffithuni.edu.au (A.R. Zarifsanayei).

https://doi.org/10.1016/j.coastaleng.2022.104080
Received 21 June 2021; Received in revised form 15 October 2021; Accepted 2 January 2022
Available online 5 January 2022

quantified in LST estimations (e.g., Kroon et al., 2020). Forcing conditions and LST models are the main sources of uncertainty in LST estimations (Murray and Antolínez et al., 2019; Zarifsanayei et al., 2020). In recent years, different hindcast datasets of offshore waves and wind forcing have become available on a global scale (e.g., ERA5, Hersbach et al., 2020; CAWCR, Smith et al., 2020). As the datasets are generated with different wave modelling frameworks forced by different wind fields, each dataset might present a different pattern of offshore waves. Offshore waves should be translated to nearshore forcing using spectral wave models. The effect of local wind on wave transformation can also be considered in the same manner. However, the high computational costs of spectral models are generally prohibitive for simulation of full time series of waves and local winds. To overcome this issue, different approaches such as traditional binary look-up tables (e.g., Vieira Da Silva et al., 2018), energy flux method (e.g., Benedet et al., 2016) and machine-learning-based techniques (e.g., Antolínez et al., 2016) have been developed for calculating wave transformation with reasonable computational costs (see de Queiroz et al., 2019 for more details). The obtained nearshore wave forcing could be introduced to different classes of LST models, including bulk formulae (e.g., Shaeri et al., 2020) and process-based models (e.g., Tonnon et al., 2018), to estimate variations of littoral drift in time and space. It should be noted that addressing all the main sources of uncertainty in sediment transport studies is normally overlooked, and as a result the level of confidence of the estimations is not presented. Scrutinizing the uncertainty is also important for climate change-driven coastal erosion studies, where uncertainties from different sources accumulate and eventually can question the reliability of any management decisions made accordingly (Le Cozannet et al., 2019; Morim et al., 2019; Ranji et al., 2022; Toimil et al., 2020).

This paper aims to quantify main sources of uncertainty when estimating the annual and seasonal patterns of LST rates, at the Gold Coast, southeast Queensland, Australia. An ensemble of LST estimations is developed to account for the uncertainty associated with the choice of hindcast forcing datasets (FD), nearshore wave transformation methods (WT) and LST models (LSTM). Evolution of uncertainty across time and associated with each source is quantified using a variance-based method for seven sites along the GC. A weighted ensemble mean is also developed to investigate temporal and spatial variability of LST patterns.

2. Study area

The Gold Coast (GC) is a coastal city located in southeast Queensland, Australia (Fig. 1a). The city's unique beaches are also a major reason for the rapid development of tourism industry which is one of the main sources of local revenue. The GC has 35 kms of predominantly sandy coast stretching north from Tweed River entrance to GC Seaway (Fig. 1b). The beaches are characterised by medium to fine sand which is uniformly distributed along the coast (Mathews et al., 1998). The littoral system is interrupted by three natural headlands and four river/creek inlets. Periodic beach nourishment has been adopted as a plausible solution for coastal erosion for this area (DHL, 1992). The required sand volume for beach nourishment is usually supplied from offshore deposits, river inlet dredging, and sand bypassing/back passing. A sand bypassing system located in the proximity of the Tweed River inlet pumps sediment to several downdrift sites to decrease the risk of not only the inlet closure but also to avoid sediment deficit for the southern beaches. Another Sand bypassing system, located at the northern end of GC close to the GC Seaway, is under operation for the same reasons. The city's shoreline experiences unidirectional northward littoral drift due to the predominance of wave energy from south easterly direction. The average long-term net northward littoral drift of 635,000 m^3/year has been estimated for the northern GC by extensive sediment budget analysis supported by comparison of hydrographic surveys, rate of sand bypassing system operations, and numerical modelling (e.g., GCCM, 2017).

The deep-water wave climate of southeast Queensland is influenced by swell-wave mechanisms, normally generated in the Southern Ocean, Tasman Sea and Coral Sea; and also, sea waves generated by local winds. Long term patterns of net wave energy reaching the coast, clearly shows the predominance of southeasterly waves (Fig. 2a). The swell window is quite large and extends to the eastern Pacific Ocean. However, only very low energy from there propagates to the study area without any significant contribution to LST. Wave climate systems of this region can be

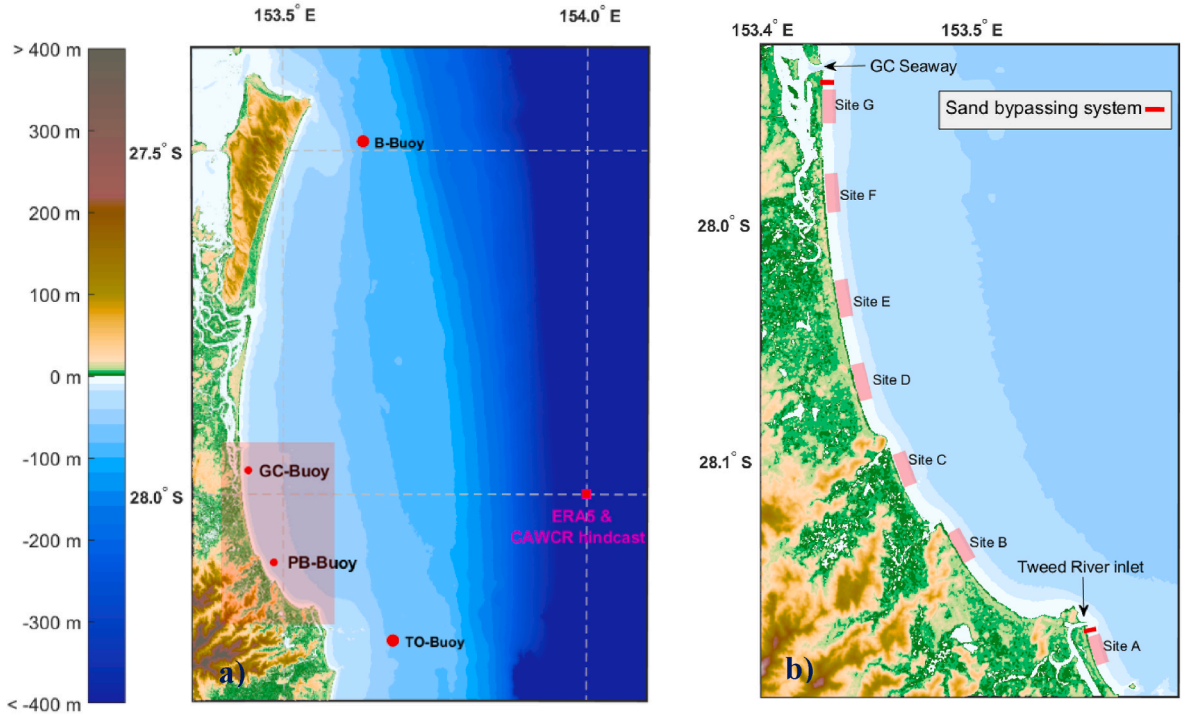

Fig. 1. a) Study area (highlighted); b) location of sites selected for LST estimations.

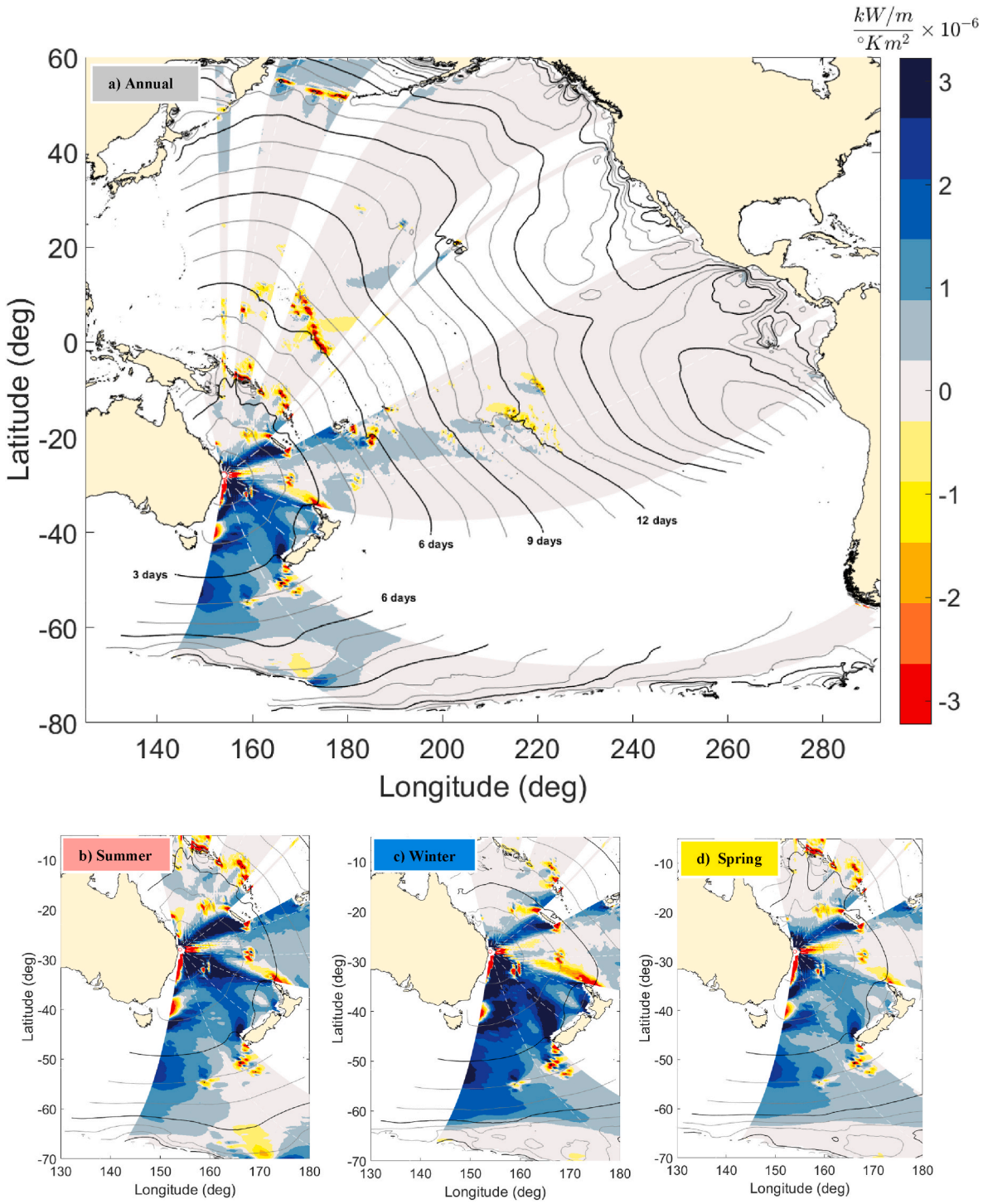

Fig. 2. Long-term footprints of net wave energy reaching offshore region of the GC at different timescales; a) Annual; b) Summer; C) Winter; d) Spring; Positive values of the color bar refer to the generation areas of wave energy while negative values refer to the dissipation areas of wave energy; Isolines show the average traveling time of the waves (following Pérez et al., 2014).

decomposed into three distinct seasons (CGC, 2015); summer (Dec to May), winter (June to Aug), and spring (Sep to Nov). The summer wave climate is characterized by consistent trade-wind swell and tropical cyclones. Moreover, swell wave energy from east to southeasterly direction exists (see Fig. 2b). During the winter season, eastern Australia is influenced by the eastward passage of intense low-pressure systems to the south, which generate moderate to high energy south to southeast swell (see Fig. 2c). Intense low-pressure systems known as East Coast Lows (ECL's) also develop in the Tasman Sea and rather than tropical cyclones, ECL's are responsible for most of high wave energy events of southeast Queensland. The spring season wave climate is calmer compared to the other seasons. This is due to a reduction in swell wave energy (reduction in frequency of ECL's) from south to southeasterly directions. Rotation of wave energy toward a more easterly direction is also conceivable (see Fig. 2d). Local wind seas are generated in different seasons (particularly during summer) and can combine with swell waves and may also approach the coast from a different direction to swell.

The exposure of GC beaches to the wave climate varies from south to

north mainly due to coastal curvature along the shoreline. The northern GC has open beaches which are generally east facing. The southern GC beaches are semi embayed beaches (zeta-shaped coastline) which curve strongly to face northeast to north. All parts of GC beaches are vulnerable to swells from the east to northeast direction. Contrary to the northern GC beaches, the southern GC beaches are less exposed to the dominant southeasterly swell direction (due to sheltering effects). Additionally, the relatively narrow width of the continental shelf can refract the dominant southeasterly swell waves significantly. Broadly speaking, refraction and sheltering effects can also result in an increasing wave height from south to north of the GC.

The focus of this paper is seven sites covering south to north of GC shoreline. The sites were selected to investigate uncertainty in LST estimation (Fig. 1b). All sites are relatively located far from the coastal structures and headlands. One site is located in updrift of the Tweed River sand bypassing system (site A), two sites are located in the semi-embayed coasts (sites B and C), one site is located at the middle of GC (site D), and three sites are located in open coasts of northern GC (sites E, F, and G).

3. Methodology

3.1. Overview of the modeling framework

In this study, an ensemble modeling framework consisting of two different forcing conditions, two wave transformation methods, and eight LST models were employed to estimate LST rates at seven sites along the GC shoreline. The modeling framework is outlined in Fig. 3.

3.2. Datasets of forcing conditions

Generally, data from different sources such as hindcast projections, wave rider buoys, and satellite can be used as offshore wind and wave forcing conditions. Although it is preferable to use the measurements to estimate LST patterns, the data are limited to specific sites, specific parameters (e.g., significant wave height, H_s) and they usually do not present long-term continuous time history. Due to the aforementioned limitations in the measurements, usually, wave information from wave hindcast projects can be of interest to coastal engineers. Several global wave hindcasts have been developed in the last decade using different wind forcing and wave models' settings. Prime examples of such data sources are CAWCR (Center for Australian Weather and Climate Research; Smith et al., 2020) and ERA5 (the fifth generation of ECMWF -European Centre for Medium-Range Weather Forecast- atmospheric reanalyses of the global climate; Hersbach et al., 2020).

The CAWCR hindcast dataset has been developed by CSIRO (Commonwealth Scientific and Industrial Research Organisation) with the primary objective of generating global data on a coarse resolution spatial grid of 0.4 deg, and higher resolutions of 4 arc minutes and 10 arc minutes for the Australian and central and south west Pacific region

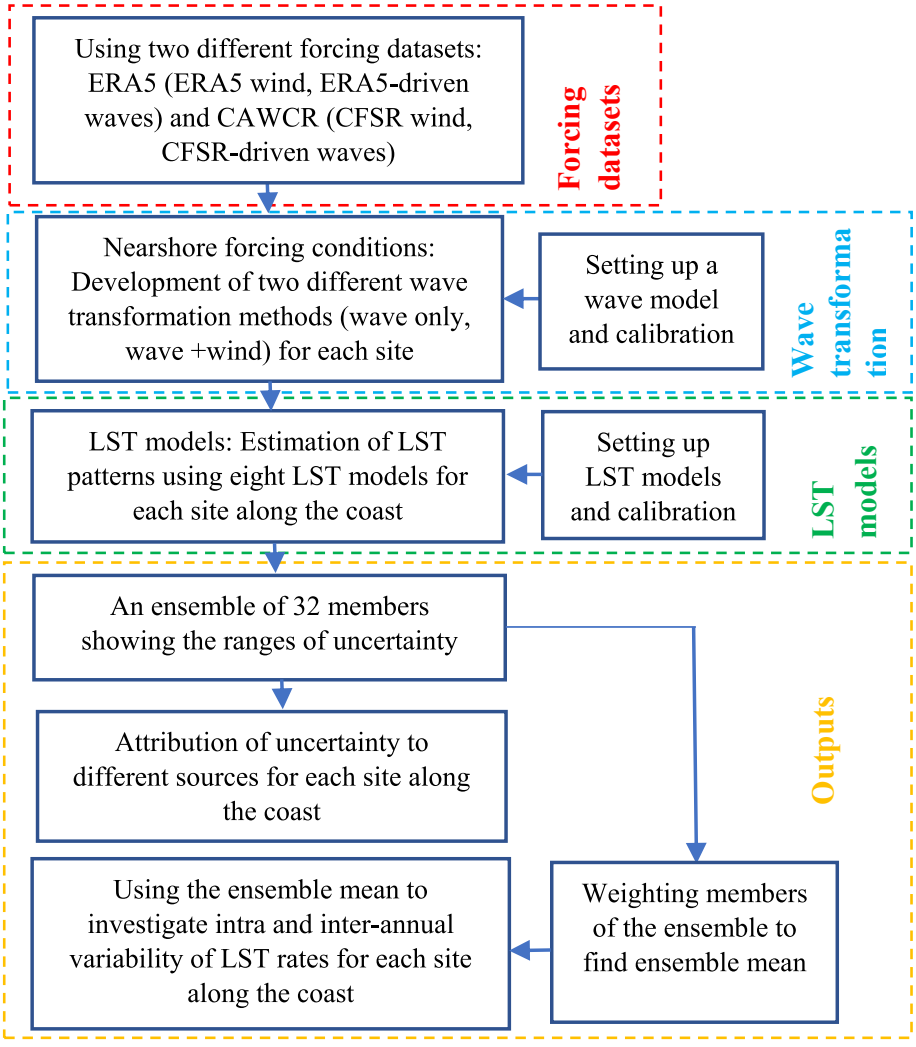

Fig. 3. Modelling framework.

(Durrant et al., 2014; Smith et al., 2020). Wind forcing data for the CAWCR hindcast were extracted from CFSR (Climate Forecast System Reanalysis, Coverage 1979–2011, with a spatial resolution of 0.3°) and CFSv2 reanalysis (coverage 2011-present, with a spatial resolution of 0.2°) which have an hourly temporal resolution. In the CAWCR project, the third-generation wave model WAVEWATCH III (Tolman, 1991) was driven with the surface wind fields (obtained from the sources mentioned before). The main outputs of CAWCR at the global resolution are integral wave parameters of total wave energy (e.g., H_s, peak wave period T_p, mean wave direction D_m), wave parameters for four partitions (three partitions for swell and one partition for sea waves), and also wind parameters.

ERA5 is a climate reanalysis dataset developed by ECMWF, covering the time slice 1979 to present, whose outputs are re-gridded with a spatial resolution of 0.25° and 0.5° for atmosphere and ocean waves, respectively. ERA5 reproduces wind fields, particularly during stormy conditions, more precisely than the dataset of ERA-Interim (e.g., Belmonte Rivas and Stoffelen, 2019). As a result, more reliable wind fields are used for the ocean wave simulations carried out using the WAM model (Hasselmann et al., 1988). Similarly, to CAWCR, integral parameters of total wave energy, as well as wave parameters of three swell partitions and one wind sea partition, and wind parameters are the main output data.

In this study, wind and wave parameters from ERA5 and CAWCR (with spatial resolution of 24 min for waves) datasets for the time slice 1979–2020 were extracted. This way, different datasets from different modelling frameworks with more or less the same resolution were utilized. Wave data of a grid point close to the study area located in deep water, were used as the boundary condition of a wave model (Fig. 1a and Table 2). Wind data for the nearest grid points to GC (wet grids) were extracted and averaged (see part A of the supplementary).

The nearest co-located grid points of ERA5 and CAWCR datasets, and Brisbane buoy (located at the depth of 70 m) were chosen to calculate the accuracy metrics for onshore directed waves ($180 > \theta > 0$) for the period 2000–2020 (Table 1). More details about comparison of the hindcast datasets with the Brisbane buoy data through drawing long-term pattern of mean energy flux on a polar coordinate system, and also QQ-plots are available in part A of the supplementary. Moreover, wind roses of ERA5 and CFSR were qualitatively compared with that of GC Seaway automatic station, and they were in reasonable agreement (not shown).

From monthly averaged wave parameters of ERA5 and CAWCR datasets, some valuable information was obtained (Fig. 4a and b). First, three distinct seasons (i.e., summer, winter, and spring) for wave climate do exist. During the summer season, monthly mean wave height is higher, and monthly averaged wave direction varies from east to south easterly direction. From the beginning of the winter season, wave height decreases slightly, while monthly averaged wave direction tends to remain within the south-easterly direction. When spring starts, there is a reduction of wave height, and rotation of monthly averaged wave direction from south-easterly to east is evident. Although, general patterns of waves on a monthly scale -observed in both datasets of ERA5 and CAWCR- are consistent, different magnitudes for wave parameters (particularly for wave direction) are reported. Such differences at the offshore boundary condition of a wave model might lead to a more significant difference in estimation of nearshore waves.

Table 1
Accuracy metrics of ERA5 and CWCAR waves with respect to Brisbane Buoy.

Parameter	Datasets	Correlation Coefficient (R)	RMSE	BIAS
H_s (m)	ERA5	0.89	0.32 m	−0.04 m
	CAWCR	0.88	0.37 m	0.14 m
T_p (sec)	ERA5	0.57	1.89 s	−0.3 s
	CAWCR	0.55	1.94 s	−0.12 s
D (deg)	ERA5	0.67	31 deg	−7.5 deg
	CAWCR	0.71	29 deg	−5.5 deg

Table 2
Comparison of significant wave height distribution from two datasets of ERA5 and CAWCR (1979–2020) at offshore boundary of the wave model.

Datasets	H_{s100}	H_{s99}	H_{s95}	H_{s50}
ERA5	7.40 m	3.95 m	2.96 m	1.65 m
CAWCR	8.08 m	4.18 m	3.09 m	1.68 m

Monthly averaged wind parameters show that the wind speed of CAWCR is at least 5% more than that of ERA5 (Fig. 4c and d). Moreover, hindcast monthly averaged wind direction from both datasets are somewhat different. Both datasets show that during summer, wind and offshore wave directions are nearly in line. But during spring, most of the time, the angle between monthly averaged wind and wave is large (>40 deg). Seasonal wave and wind roses are also available in part A of the supplementary.

3.3. Wave transformation

3.3.1. Wave model set-up and calibration

In this study a hybrid method for downscaling of offshore waves to the nearshore area was employed. The method first requires a calibrated wave model (Mike 21 SW) for transformation of some samples (and/or the centroid of clusters) of offshore waves to the nearshore. Mike 21 SW is a third-generation spectral wave model, it is capable of simulating the generation of waves by winds, dissipation by white capping, depth induced wave breaking, bottom friction and wave-wave interaction in both deep and shallow water (DHI, 2017). The model was previously used successfully for the GC region to simulate wave and sediment transport (e.g., Splinter et al., 2012).

Fig. 5 indicates the computational domain of the model with the main open boundary located at east extended to north and south, two lateral boundaries located at north and south, and a closed (land) boundary located at west. To minimize the effect of inaccurate lateral boundary conditions, the domain was created with sufficient distance on either side.

To ensure the mesh size does not impact the patterns of LST, the following steps were taken. Different wave models were set up by changing the mesh size. Each wave model was forced with a subset of 350 characteristic wave boundary conditions extracted from the joint ERA5 and CAWCR wave datasets (H_s, T_p, D_m).The subset was extracted from the datasets by first applying the Maximum Dissimilarity Algorithm (MDA), and then K-mean Algorithm (MKA) (Camus et al., 2011b). The MDA reduced the size of the original dataset to 1/10 while distributing wave conditions more uniformly. Then, the KMA was more capable of capturing both extreme and modal wave climate to cluster wave data. For each setting of the wave model (different mesh size), the centroids of clusters were transformed to nearshore regions at 15 m water depth (depth of closure) for the seven sites mentioned in the previous section. Waves from that water depth were transferred to the breaking point using Larson et al. (2010) formula. Then LST rate was calculated using the most recent bulk formula of Shaeri et al. (2020). Knowing the probability of occurrence of each cluster, long-term average annual net LST rate for each site along the coast, associated with each wave model setup, was then estimated. When a new model setup (with new mesh size) had a marginal influence on the LST rate for each site, the analysis was stopped. At the final step of mesh size sensitivity analysis, the number of required grids was 8500 to generate varying mesh sizes (i.e., 12 km^2 at offshore region reaching 0.0045 km^2 in nearshore). The same steps were taken to find the required number of bins for directional discretization of wave energy equation in Mike 21 SW. It was found that 50 bins covering 0–360° suffices for accurate wave simulations.

The wave model was calibrated in two steps. At the first stage of the model calibration, eight months wave data from offshore buoys

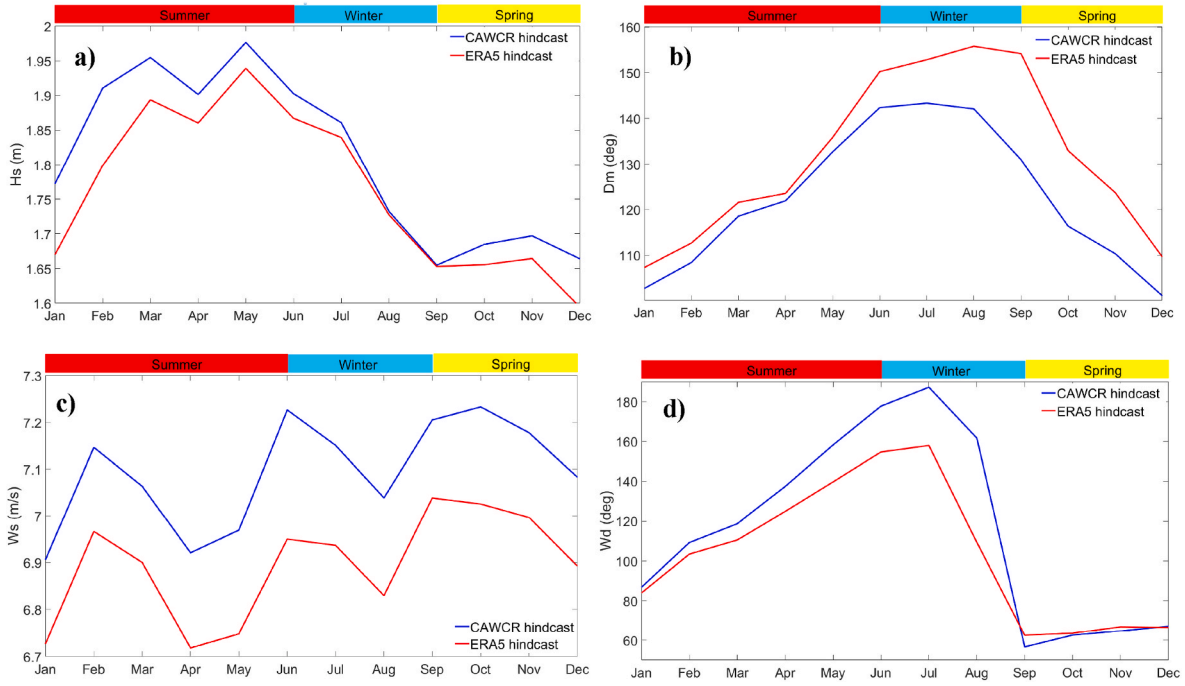

Fig. 4. Monthly mean of wind and wave parameters; a) monthly averaged significant wave height; b) monthly averaged mean wave direction; c) monthly averaged surface wind speed; d) monthly averaged surface wind direction; The whole time series of the forcing conditions, summarised in this figure, were employed for wave simulations.

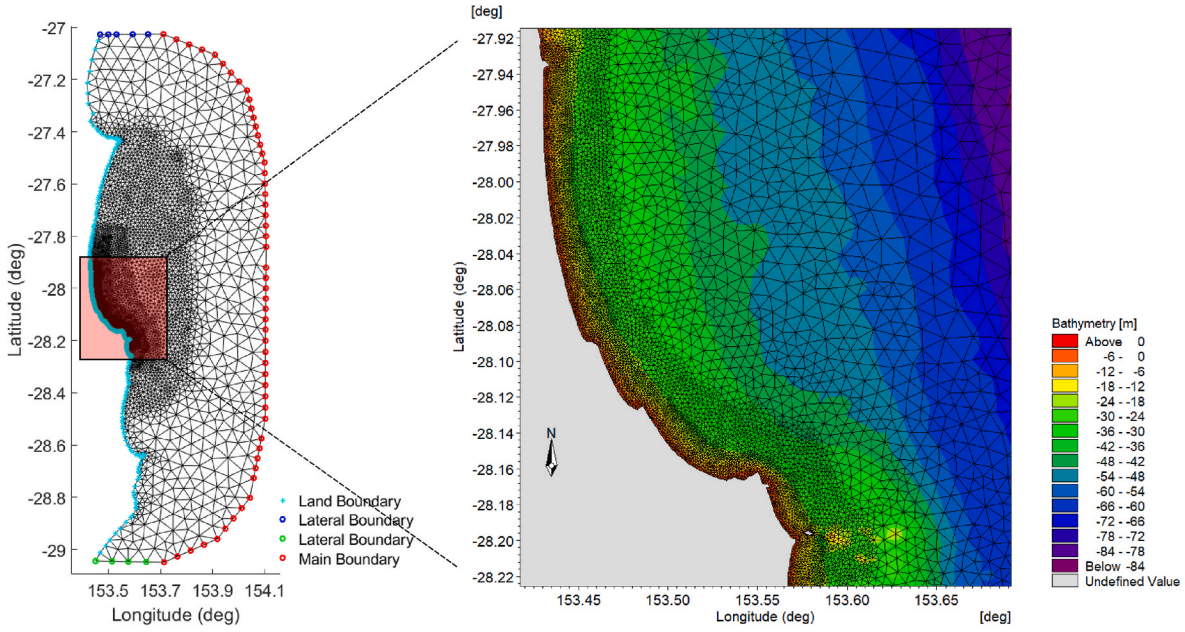

Fig. 5. Left: Computational domain; Right: the area of interest.

(Brisbane (BB) and Tweed offshore (TOB) wave buoys data for the time slice Feb 2020 to Sep 2020) were used as the boundary condition of the wave model. At this stage, no wind forcing was considered as the boundary condition of the wave model was obtained from the buoys that have been already influenced by local wind energy. The results of wave simulations were compared with two nearshore wave buoys data (Gold Coast (GCB) and Pam beach (PBB) wave buoys) to tune directional standard deviation and bed friction parameter. Fig. 1a indicates the location of the buoys used in this study. At the next stage of the model calibration white capping parameters were tuned. To do so, wind and wave forcing conditions obtained from CAWCR datasets (with a resolution of 4 min), were used. The model was run for two periods Jan–Feb 2013 and May–June 2009 when significant wave forcing from the offshore region along with local wind resulted in two extreme conditions accompanied with waves higher than modal conditions (i.e., Hs $>$ 1.7 m). The results of the simulations were compared with the GC Buoy data. More details about wave model calibration can be found in part B of the supplementary.

3.3.2. Reconstruction of nearshore waves of CAWCR and ERA5 datasets

Different approaches such as the energy flux method, K-mean algorithm (KMA), and traditional look-up tables have been used for this case study to transform offshore waves to nearshore ones (Faivre et al., 2017; Splinter et al., 2011; Vieira Da Silva et al., 2018). In all of the methods some samples/centroids of clusters are selected and used as the boundary condition of a spectral wave model. The energy flux method cannot properly capture the patterns of storms conditions as the approach provides the average of each group as a function of wave energy distribution. However, due to its simplicity, it is popular. Clustering approaches like K-mean are capable of condensing large data in a multidimensional space (e.g., H_s, T_p, D_m). However, they suffer from missing the data located at the edges of the cloud of data (e.g., extreme conditions). Hence, this strategy usually underestimates extreme conditions and overestimates calm conditions. To overcome this issue, the forcing parameters can be weighted (see de Queiroz et al., 2019) to push the algorithm to a side of the cloud of data (e.g., towards extreme conditions) with the risk of missing data located at the other side of cloud of data (e.g., calm conditions). The performance of traditional look-up tables is usually dependent on the samples selected as the boundary condition of a wave model. In this method nearshore wave time series are reconstructed using multi linear interpolations. Although increasing the number of bins could improve the skill of traditional look-up tables, this leads to unmanageable/infeasible computational costs particularly if both wave and wind parameters are being considered. For instance, the number of required wave simulations assuming 10 bins for wave height, 8 bins for wave period, 15 bins for wave direction, 5 bins for wind speed, 5 bins for wind direction is 30,000. Also, it should be noted that in previous studies the effect of local wind on nearshore waves was overlooked. Since the relation between sediment transport and wave forcing is nonlinear, errors in wave transformation can develop uncertainty of estimated LST patterns remarkably.

To reconstruct the whole time series of nearshore waves with a more reliable approach, two promising alternatives were tested. The first one aims to create a look-up table of characteristic wave conditions, as described in 3.3.1. The second one consists of training a surrogate model for wave transformations (Camus et al., 2011a). The surrogate model is built on three steps. First, a subset of characteristic wave boundary conditions is selected. Second, stationary wave transformations using a spectral wave model are carried out on this subset. And third, non-linear interpolation techniques are used to reconstruct nearshore wave time series. In this regard, sampling with the MDA algorithm and interpolating with Radial Basis Functions (RBF) has been shown successful to investigate wave-induced sediment transport (Antolínez et al., 2018, 2019).

After checking the accuracy of each alternative, it was decided to follow the second approach (i.e., wave transformation through a surrogate model). Then, nearshore waves associated with the following forcing conditions were reconstructed:

a. Wave conditions at offshore boundary without local wind effects (hereafter WT1), and
b. Wave conditions at offshore boundary plus wind forcing (hereafter WT2).

In this way, inclusion/exclusion of local wind impacts on wave growth was treated as the uncertainty of the wave transformation process.

Generally, an issue for reconstruction of nearshore waves and estimation of the corresponding LST patterns is the way by which the boundary conditions are defined. Usually, integral parameters (i.e., H_s, T_p, D_m) associated with total wave energy are chosen and then converted to a single peak wave density spectrum format. However, mixed sea states (multi-modal conditions) can change the shape pf spectrum from single peak to multiple peaks. It should be pointed out that addressing uncertainty arising from working with integral parameters versus sea-swell partitions is beyond the scope of this paper. Hence, in this paper, the assumption of having a single peak spectrum at the boundary condition of the wave model was adopted. More details about mixed sea states of GC can be found in part C of the supplementary.

Given the abovementioned assumptions, the steps of Fig 6 were taken to convert time series of offshore wave parameters of H_s, T_p, D_m, and wind speed W_s and wind direction W_d to nearshore waves time series at each site along the GC shoreline. The reconstructed nearshore waves were validated against the calibrated wave model (Mike 21 SW) for all sites (in part C of the supplementary the performance of the wave reconstruction method at site D was presented).

3.4. LST models: set-up and calibration, and LST estimates

Two classes of LST models (i.e., bulk formulae and process-based models) were employed to provide an ensemble of outputs. Four bulk transport formulae, including modified CERC (Mil-Homens et al., 2013; hereafter MC), modified Kamphuis (Mil-Homens et al., 2013; hereafter MK), van Rijn (van Rijn, 2013; hereafter V) and Shaeri et al. (2020) (hereafter S) were selected. Each formula presents a different level of sensitivity to different parameters (see also part D of the supplementary). Hence, it is worth using all of them to capture a wide range of uncertainty in LST estimations.

Apart from the bulk formulae, the process-based model DHI-LITPACK (hereafter DHI) which accounts for the shape of coastal profiles (i.e., nearshore bathymetry), was used. The model has a number of factors to control the estimate of LST rate. Hence, an extensive sensitivity analysis was conducted in advance. To do so, a short stretch of coastline close to the GC seaway (site G) was chosen. Coastal profiles measured since 1966 (not measured on a regular basis) for this region was analyzed to choose three coastal profiles that could be representative of a no-sand bar profile, a significantly eroded one, and a profile in transition between severe erosion and recovery (see part D of the supplementary). Forcing conditions for the model were obtained from the GC buoy for the period 2008–2020, when directional wave parameters were available. The sensitivity of the model to the most important settings can be found in the supplementary part D.

Since the focus of this paper is on long-term patterns of LST, choosing a representative bathymetry to set up the process-based model, was a challenge. Although in the literature, it is common to take one of the hydrographic surveys (i.e., measured profiles) as the bathymetry of model (e.g., Bonaldo et al., 2015), the applicability of such a strategy for study of long-term patterns of coastal sediment transport is debatable. To address this issue, a synthetic equilibrium barred beach profile following Holman et al. (2014) was developed. To do so, available hydrographic surveys were analyzed to find the mean position of the main bar crest and seaward limit of main bar for each location along the coast. All coastal profiles (except the ones measured after extreme conditions), were used for fitting the equilibrium barred profiles. The developed synthetic bathymetry preserves the main features of coastal profiles along the GC shoreline, including the existence of an outer sand bar with the mean position of 150–200 m measured from shoreline, seaward limit of sandbars located in water depth 5–6 m, and an average beach slope of 0.025. As for this case study, almost in all seasons, stormy conditions occur (see part A of the supplementary), no clear/significant seasonality effect on the position of main bar was observed in the available hydrographic surveys. Although during spring season the wave climate is relatively calmer than the other seasons, the occasional occurrence of storms, rotation of waves toward more easterly direction, and the limited time for recovery (about three months) restrict the occurrence of recovered profiles. Hence, for each site along the coast, only one equilibrium barred profile was fitted to the measured profiles (e.g., see Fig. 7 for site G).

Regarding the shoreline orientation, mean sea level was adopted as shoreline proxy, and average of long-term coastline orientation obtained from hydrographic surveys and satellite images (post processed by

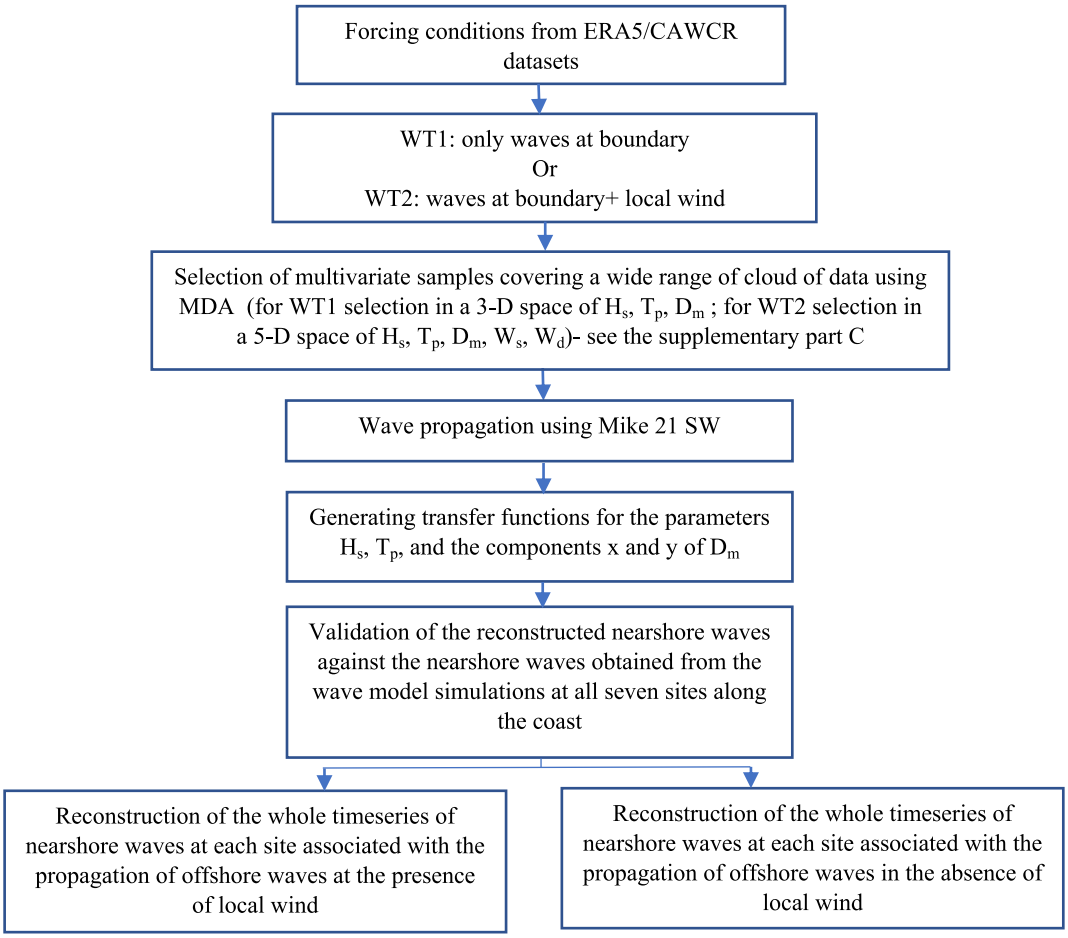

Fig. 6. Flow chart of nearshore wave reconstruction.

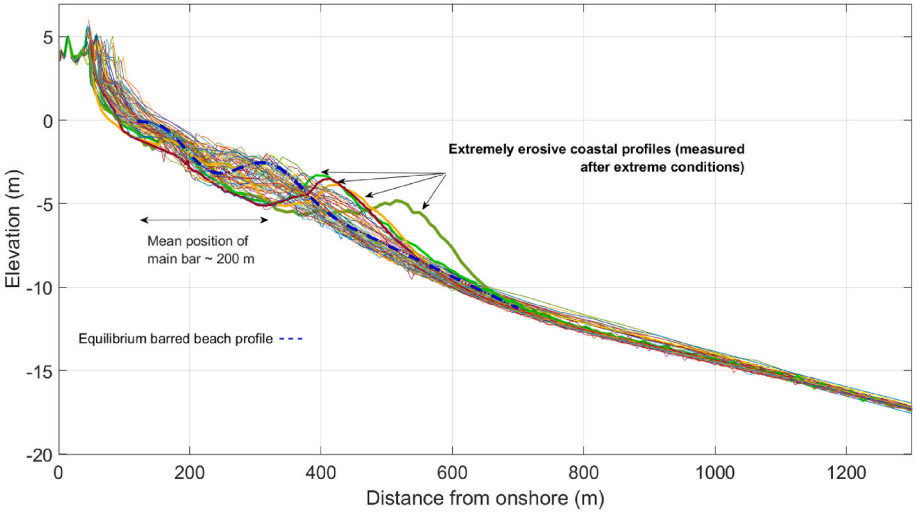

Fig. 7. Equilibrium barred beach profile fitted to the measured coastal profiles at site G.

Bishop-taylor et al., 2021), were used in this study (see supplementary part D).

The GC buoy data, covering the time span 2008–2020 was used as the forcing condition for each LST model to reproduce the estimated average long-term annual net LST rate of 635,000 m^3/year (GCCM, 2017) for the northern Gold Coast (site G). For calibration of the bulk transport formulae, simple adjustment factors were applied; while for calibration of the process-based model, its free parameters were tuned (see part D of the supplementary). To transform GCB wave data to the breaking zone, depth-induced breaking wave height was estimated using the breaker index (γ_b) of Kamphuis (2010):

$$\gamma_b = H_{sb}/d_b = 0.56\, e^{3.5m} \quad (1)$$

where H_{sb} is breaker height, d_b is the water depth at breaking point, and

m is the average surf zone bed slope. Moreover, for the DHI model, the wave motion outside boundary layers was estimated using the non-linear wave theory of Doering and Bowen (1995). This semi empirical theory is valid for both breaking and non-breaking waves. The DHI model calculates bedload through the empirical approach of Zyserman and Fredsøe (1994) or the deterministic approach of Engelund and Fredsøe (1976). Both approaches were used as the model was sensitive to the choice of bedload description. Moreover, according to Ostrowski (2016) suggestions, each bedload description was combined with non-graded and size-graded sediment transport modeling. Finally, four different set-ups of the DHI model were used (see part D of the supplementary). In this way, process-based models (one model with different set-ups) along with four bulk formulae were used to avoid bias against the results of any class of models for ensemble modeling.

The calibrated LST models were then forced with the reconstructed nearshore waves of CAWCR and ERA5 datasets (transferred with WT1 and WT2) to estimate LST patterns at each of seven sites along the coast. Among the sites, site A is more vulnerable to changes in shoreline orientation due to interaction of management scenarios and natural processes. Hence, for this site, relationship between shoreline orientation and annual mean LST rate under different forcing conditions (i.e., S-Phi curve) was also calculated (see supplementary part E).

3.5. Contribution of each source of uncertainty to total uncertainty

The ensemble modelling yields a set of results showing LST rate variations in time and along the coast. Here, it was aimed to decompose total ensemble uncertainty into the main sources of uncertainty and their interactions. To do so, following Morim et al. (2019), the variance-based method of ANOVA was used. To improve the reliability of ANOVA method and decrease the bias in estimates of variance sources, following Bosshard et al. (2013) a subsampling scheme was adopted beforehand. In each subsampling iteration n, two FDs, two WTs, and two LST models were considered and introduced to ANOVA model. Given three predefined factors of uncertainty in LST estimations, the following three-factor ANOVA model without replication was employed for each subsample:

$$LST^{n}_{ijk} = \mu^{n} + FD^{n}_{i} + WT^{n}_{j} + LSTM^{n}_{k} + int\,(FD, WT\,)^{n}_{ij} + int(FD, LSTM)^{n}_{ik} + int(WT, LSTM)^{n}_{jk} + int(FD, WT, LSTM)^{n}_{ijk} \quad (2)$$

where LST_{ijkn} is an observation of the response variable (here LST rates) in subsample n. μ^{n} is the overall mean of the LST rate in subsample n. FD_i, WT_j, and $LSTM_k$ are the variance arising solely from the individual factors FD, WT, and $LSTM$, with i, j, and k denoting samples of different factors ($i = 1,2$, $j = 1,2$, $k = 1,2$) for each subset of simulations by a combination of two FDs, WTs, and $LSTM$s. Terms 'int' shows interactions between the specified factors. Note that the inputs of ANOVA method can be introduced with different time formats (e.g., monthly, seasonally, yearly) to investigate the contribution of each source of uncertainty in total variance that varies in time. The results extracted from each subsample n (i.e., variance of each source divided by total variance) are summed and averaged to present the mean unbiased estimates of fraction of the total uncertainty attributable to each source.

3.6. Weighting the members of the ensemble

The ensemble of results was presented by 32 members (e.g., CAWCR (as the forcing dataset)+WT1 (as the wave transformation)+S (as the LST model) = LST estimations associated with member #1) that might have different performance. Hence, finding a weight for each member of the ensemble was required. A weighted average estimation of LST rate was obtained by using the accuracy of each member relative to the reference LST data. Following Marsooli et al. (2019), a weighting factor was assigned to each member of the ensemble, based on quantitative model skill of Willmott (1981):

$$MSE_i = \left\langle (m_i - r)^2 \right\rangle \quad (3)$$

$$S_i = 1 - MSE_i \Big/ \left\langle \left(|m_i - \langle r \rangle| + |r - \langle r \rangle| \right)^2 \right\rangle \quad (4)$$

$$W_i = S_i \Big/ \sum S_i \quad (5)$$

where m_i represents LST rates associated with the member i of the ensemble, r is the reference LST data, MSE_i is mean square error, $<>$ denotes a mean, S_i is the Wilmott skill score ($0 < S_i < 1$), W_i is the weight assigned to the member i. Note that the annual LST rates at site G (2008–2020), obtained from each calibrated LST model under forcing conditions of GC, were used as the reference LST data for weighting each member of the ensemble.

4. Results and discussion

All LST models used in this study, could only work with integral parameters of total wave energy (not the shape of spectrum nor integral parameters from different partitions). Hence the representative wave parameters (i.e., H_s, T_p, and D_m associated with total wave energy), were employed to build a single-peak spectrum to be used as the boundary condition of the wave model. Following de Swart et al. (2020), within the wave parameters of hindcast datasets, D_m can be a decent representative of wave direction for the reconstruction of a single peak wave spectrum, as D_m is influenced by both sea and swell partitions of wave energy. D_m in combination with DSD parameter can control the directional pattern of total wave energy approaching the coast. Hence, to choose more reasonable parameter for wave spectrum, the DSD parameter was also tuned. A DSD value of 35 deg was finally adopted, implying that a narrow-banded spectrum (e.g., a swell dominated spectrum) cannot be considered for this study area. In this way, the effect of both partitions of the sea and swell on the representative offshore waves, wave transformation, and the resulting LST were considered implicitly through parameters D_m and DSD of total wave energy.

The results of nearshore wave reconstruction were employed to estimate the patterns of wave attenuation (i.e., relationship between $H_{s\text{-offshore}}$, T_p, $D_{m\text{-offshore}}$ and $H_{s\text{-nearshore}}$) when offshore waves approach the coastal sites. Fig. 8 shows wave attenuation patterns for site D associated with two cases of CAWCR + WT1 and CAWCR + WT2. As shown, for case CAWCR + WT2, most often lower magnitude of wave attenuation is observed, compared to the case CAWCR + WT1. The negative values of Fig. 8c and 8d belongs to the waves captured wind energy remarkably that resulted in $H_{s\text{-nearshore}}/H_{s\text{-offshore}}>1$ (in part C of the supplementary the relation of $H_{s\text{-offshore}}$, T_p, $D_{m\text{-offshore}}$ and $H_{s\text{-nearshore}}$ is shown for sites A, B, and G).

Fig. 9a indicates the average of wave attenuation patterns along the coast (for case CAWCR + WT1). It implies that the existence of an embayed beach at south GC connecting to an open coast at north has caused nearshore wave conditions varying along the coast. Offshore waves from N to NE directions experience the same attenuation nearly at all nearshore sites; the percentage of wave height reduction varies from 50% to 20% when offshore waves change from N to NE direction. With the rotation of offshore waves from NE to E direction, less wave attenuation was observed in northern GC compared to the southern GC, as normal to the coastline (nearshore contours) is toward east direction and waves do not experience much refraction. However, almost at all sites, the amount of attenuation did not change much in response to the rotation of offshore waves from NE to E direction. For offshore waves approaching the coast from SE swell direction, strong refraction and sheltering of southern GC sites (particularly B, and C located at downcoast of a large headland), has resulted in a significant decrease in wave height; the percentage of wave height reduction varies from 35% to 55% when offshore waves deviate from E to SE direction. But for northern GC sites (e.g., sites E, F, and G), the observed wave height reduction was

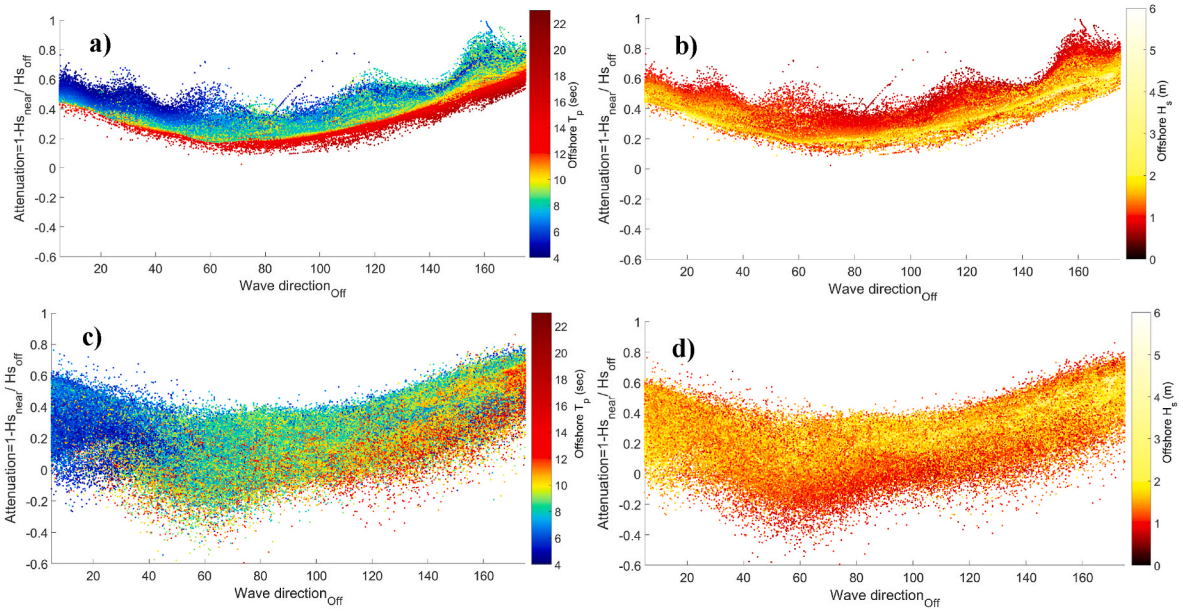

Fig. 8. Wave attenuation patterns at site D observed in whole time series of nearshore waves; a, b) case CAWCR + WT1; c, d) case CAWCR + WT2.

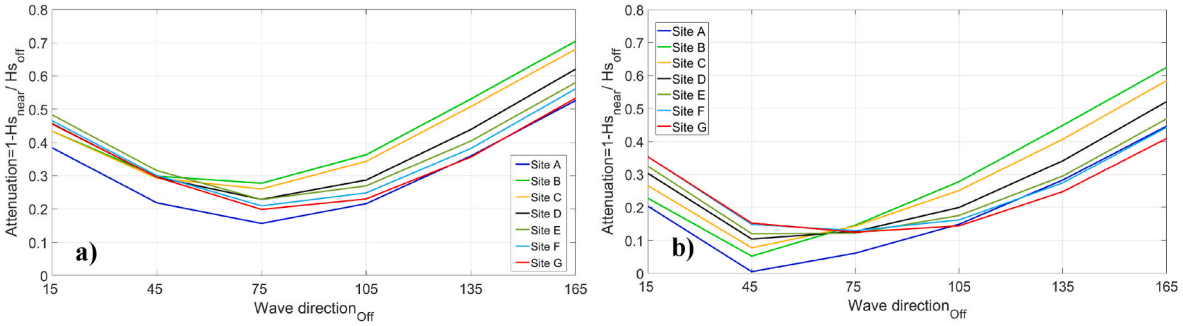

Fig. 9. Average of wave attenuation for all sites; a) case CAWCR + WT1; b) case CAWCR + WT2.

much less than the southern sites'; the percentage of attenuation varies from 20% to 45%.

The patterns of average wave attenuation in Fig. 9a were also qualitatively in good agreement with Vieira Da Silva et al. (2018) estimations, where they used Brisbane Buoy data as the boundary condition of a SWAN model, without considering the local wind forcing, to investigate wave climate variability along the GC shoreline.

When offshore waves were transferred to the nearshore zone through WT2, the wave attenuation patterns along the coast has changed (Fig. 8c, d, and 9b). On average, there was an estimation of 25% decrease of wave attenuation along the coast, compared to case WT1. This implies that by the inclusion of local wind forcing, positive net energy was supplied to the coastal system that could remarkably increase wave height along the coast and alleviate the wave dissipation due to other processes (e.g., refraction).

To examine the impacts of local wind on the temporal patterns of reconstructed nearshore waves, monthly mean wave parameters H_s and D_m were calculated for each site along the coast. Additionally, the alongshore component of energy flux was calculated to provide first impression about the potential impacts of local wind on LST patterns at all sites (see Fig. 10 for sites A, B, D, and G). Overall, at all sites along the coast, considering local wind for wave transformation resulted in a net shift (increase) of monthly mean wave height of about 10% compared to monthly mean wave height obtained from exclusion of local wind. For south GC sites (e.g., sites A, B), during January to May (summer season) the patterns of mean wave direction did not vary remarkably by including local wind. But during winter and spring seasons (July to December), the inclusion of local wind in the wave transformation, compared to the exclusion of local wind effects, caused significant changes in mean wave direction patterns (see Fig. 10, left panel). As during the spring season lower swell wave energy from southeasterly direction reaches GC beaches, given the existence of strong local wind prevailing from northeast direction during this period (see monthly averaged wind direction, Fig. 4) inclusion of local wind for wave transformation can result in the overestimation of wave height and significant rotation of waves toward a more easterly direction. Inclusion of local wind also caused an increase in the magnitude of the longshore component of energy flux at sites A, B, and C (site C not shown) during the summer season, while during spring it led to having a meagre energy flux (about zero) at these sites (Fig. 10, right panel). Zero energy flux during spring season means probably no LST. But it does not seem reasonable for site A, as this site is close to the Tweed River sand bypassing system and the system is under operation during all months of the year; however, with less pumping during the spring season. For southern GC sites, the impact of local wind on energy flux was much higher during spring, compared to northern GC. Nonetheless, energy flux at northern GC sites was mainly impacted more by local wind during summer and winter, compared to southern GC. When WT2 was employed, a larger energy flux was seen for the CAWCR dataset compared to that of ERA5. But during the spring season, using both datasets led to a similar magnitude of energy flux. Such discrepancies are due to the differences between wind field and offshore waves of

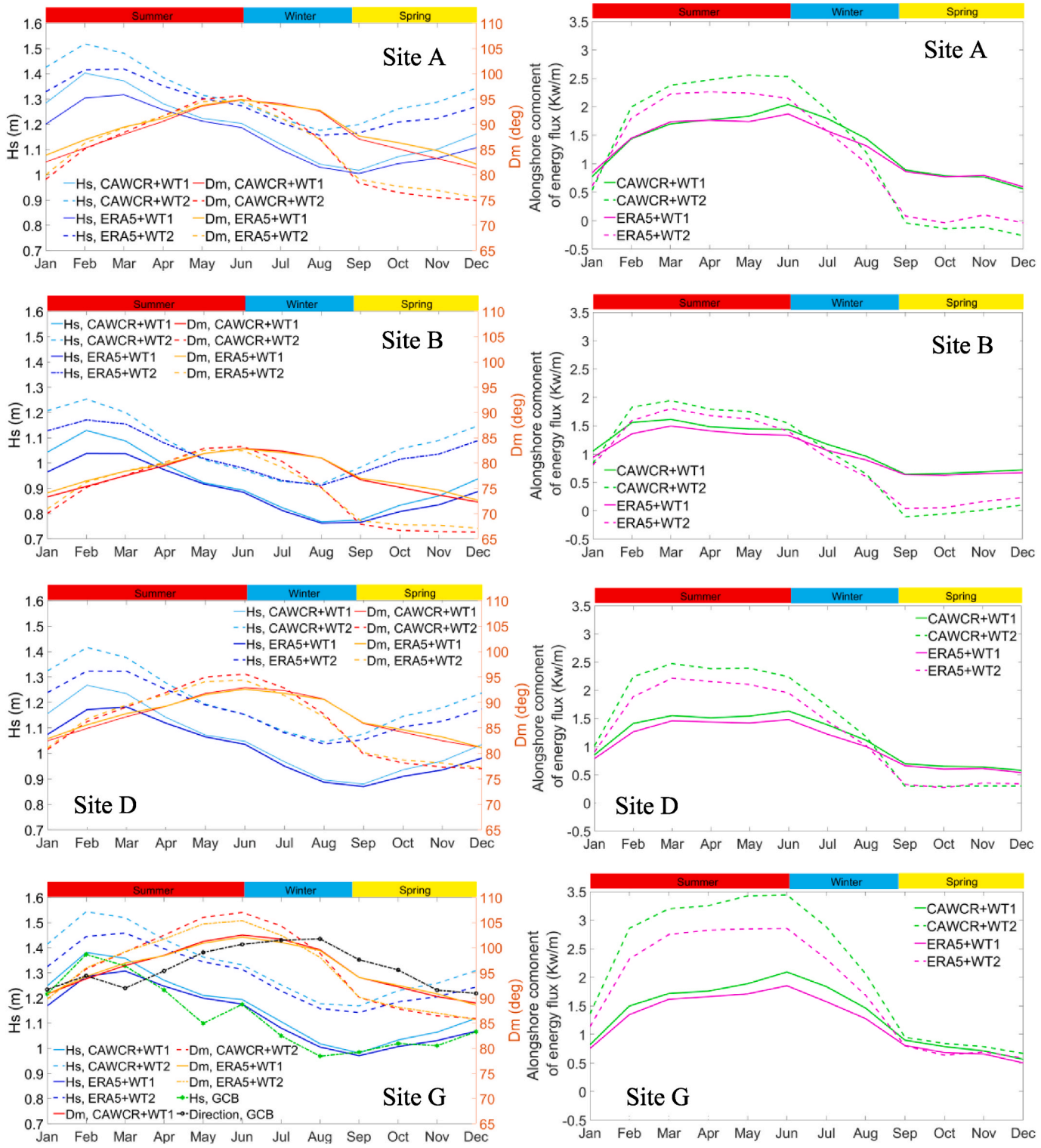

Fig. 10. Monthly mean wave parameters (left panel) and alongshore component of energy flux (right panel) variations at different sites at water depth 15 m under different forcing conditions (different datasets and wave transformation methods); At site G, monthly mean of wave parameters, obtained from GCB data, were also presented.

ERA5 and CAWCR, particularly during the winter season.

Although in this study, a rough criterion was employed for calibration of LST models (i.e., reproducing a target rate of 635,000 m3/year as long-term average net annual LST rate), use of an accurate source of nearshore wave forcing (i.e., Gold Coast wave buoy data) was beneficial to assure that the calibration was not impacted by biases of the forcing conditions. When the calibrated models were forced by nearshore waves calculated by WT1, their long-term estimations were close to each other. But forcing LST models with nearshore waves obtained from WT2 resulted in the estimations with large variance. Among the LST models, model V and DHI model (with four different set-ups) were very sensitive to changes in magnitude of wave height. Since WT2 produced larger

wave heights compared to WT1, particularly during stormy conditions, forcing the aforementioned models with nearshore waves of WT2 yield over-estimation of LST rate, compared to the rest of the models (Fig. 11b). Normally, an increasing trend in the variance of LST estimations from southern to northern GC sites was observed, implying that there is a larger uncertainty in estimation of LST rate for open coasts of the GC which should be addressed (Fig. 11a).

Judgment about the overall effect of inclusion/exclusion of local wind (i.e., WT1/WT2) on LST estimations for the GC coastal region can be challenging as the range of uncertainty in LST estimations varies from site to site and choosing one site arbitrarily to investigate the inclusion of wind/no wind effects on LST rate cannot necessarily yield reliable conclusions. Although for northern GC sites (open coasts), using WT2 together with any LST model led to an overestimating trend in mean annual LST rate, for the sheltered site B, the inclusion of local wind showed an underestimating trend. Apart from the choice of site, the LST model selection has a great impact on making the judgment. For instance, if site D was selected for judgment about the overall effect of wind inclusion/exclusion on LST estimations, by using the LST model MK/S, one might conclude that local wind inclusion leads to an overestimation of the mean annual LST rate by 10% while using LST model V and DHI-S1shows a 30% and 50% increase, respectively. Fig. 11b illustrates that at site D, for the case WT2, the variations of estimated annual LST rate obtained from all set-ups of DHI and V models were higher than those of the other models. It implies that the interaction of wave transformation method and LST models can also be a significant issue in estimations. For case WT2, the most significant overestimation of LST rate was seen at site G, where application of LST models S, MK, V, MC, DHI-S1, DHI-S2, DHI-S3, and DHI-S4 showed 30%, 33%, 75%, 45%, 240%, 290%, 270%, 230% increase in long-term annual LST rate, respectively. It should be noted that all models, for the case WT1, had presented more or less the same LST rate, but in response to the forcing obtained from WT2 their estimations became very different from each other. The magnitude and sometimes the direction of the monthly LST rates were also impacted by the choice of wave transformation methods (see part E of the supplementary). These findings are different from the previous studies where wave transformation uncertainty and its interaction with the choice of LST models were overlooked for the GC region (e.g., Sedigh et al., 2016; Splinter et al., 2011; Strauss et al., 2007).

To get more insight into the relative importance of each source of uncertainty, the variance-based model ANOVA with a sub-sampling technique was utilized for each site individually on seasonal and annual scales (see Fig. 12 and also the supplementary part F). The ANOVA model ranked the three sources of FD, WT, and LSTM, and also attributed uncertainty to the non-linear interactions of the sources, including FD-WT, FD-LSTM, WT-LSTM, and FD-WT-LSTM. On the annual scale, moving from site B to G, the relative contribution of WT to total uncertainty became significant, i.e., ~20%, 40% and 50% of total uncertainty at sites B, D, and G, respectively (Fig. 12). The increasing trend in WT uncertainty from south to north is consistent with the findings illustrated in Fig. 11a, where variations of LST estimations in response to inclusion/exclusion of local wind was presented. Almost at all sites, 30% to 50% of total uncertainty was controlled by the choice of LSTM and the interaction of WT and LSTM. At all sites, the share of other interaction sources (all interactions minus WT-LSTM) in the total variance of LST rates was meagre. The relative importance of FD in the total variance of LST estimations decreased from south to north GC.

On a seasonal scale, during summer, at all sites (except site B) the effect of wave transformation uncertainty was about 50% of total uncertainty. Almost at all sites (except site G) during winter season the uncertainty associated with the FD was more significant than those of the other sources. This can be due to the differences between ERA5 and CAWCR datasets for the parameters of wind and wave direction during winter season (see also Fig. 4). Generally, the relative importance of FD, during the winter season, from south to north decreases as WT uncertainty grows. During the spring season for southern GC sites, much uncertainty is associated with WT. As mentioned before, during this season, inclusion of local wind for southern GC sites (sites A and B) led to meagre alongshore energy flux, while exclusion of local wind resulted in a positive magnitude for energy flux (see also the supplementary part E). During the spring season, the relative importance of WT decreases for northern GC sites. This issue is also consistent with the slight differences between the patterns of alongshore energy flux associated with WT1, and WT2 (see also Fig. 10).

At the last step of ensemble modeling, a simple weight was assigned to each member of the ensemble (Fig. 13a). The smallest weights were given to the members overestimating the LST rate significantly, showing the adopted weighting scheme is working reasonably (e.g., all set-ups of DHI model and V under forcing CAWCR + WT2). Comparison of annual net LST rate obtained from the ensemble mean with the reference LST rate at site G implies that the ensemble modeling framework could generate reasonable patterns for LST (Fig. 13b).

An estimate of the monthly and annual mean LST rates, and the LST rates during non-modal conditions can be found using the weighted ensemble mean. Moreover, intra- and inter-annual variability of the LST rates (i.e., intra-annual variability: standard deviation of the monthly means/time slice mean, inter-annual variability: standard deviation of the annual means/time slice mean) can be determined with the same

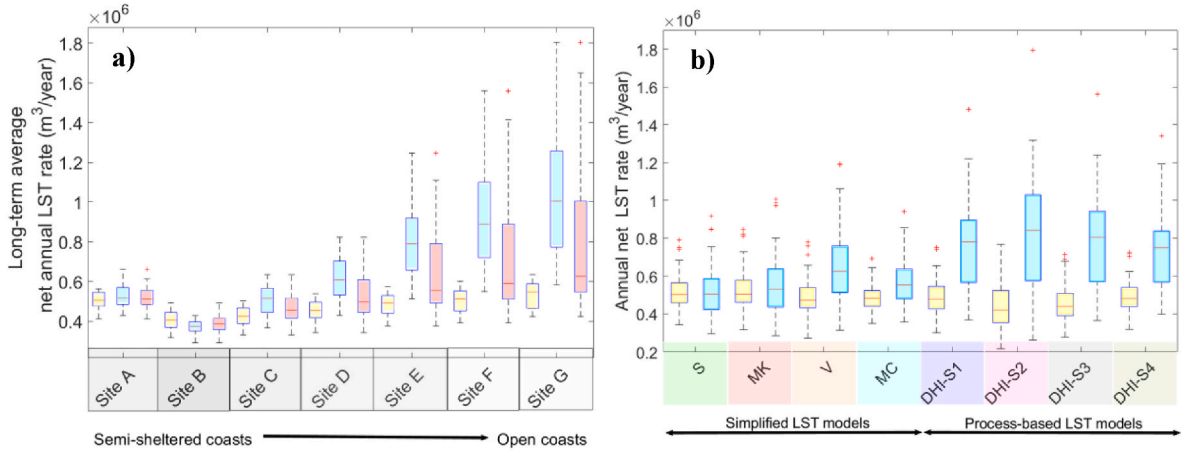

Fig. 11. a) Long-term average net annual LST rate at different sites estimated by different forcing and LST models (yellow boxes represent LST rate variations estimated by all LST models under forcing ERA5 and CAWCR datasets and WT1; blue boxes represents LST rate variations estimated by all LST models under forcing ERA5 and CAWCR datasets and WT2; red boxes represents LST rate estimated by all combination of forcing datasets, wave transformation methods and LST models); b) Annual LST rate variations at site D associated with each LST model.

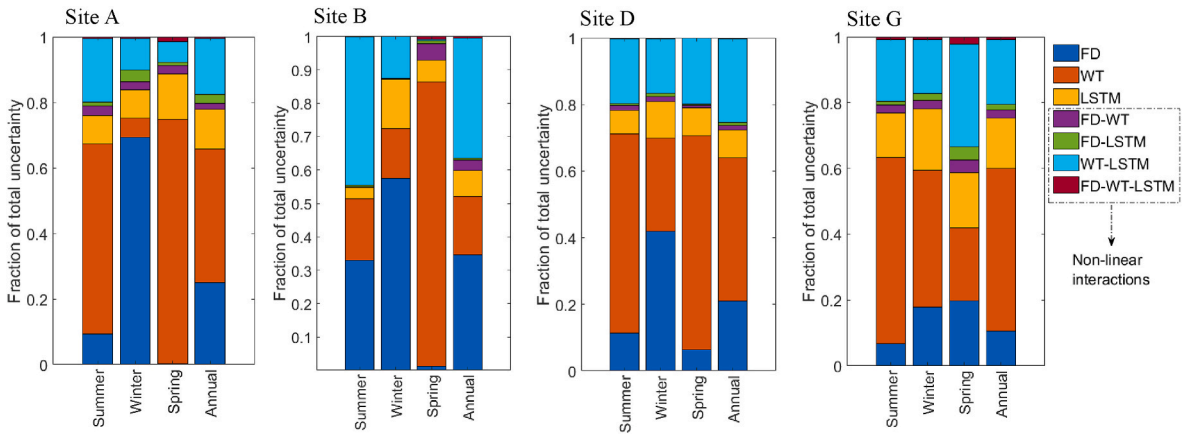

Fig. 12. Relative contribution of different sources of uncertainty in total variance of LST estimations on seasonal and annual scales at different sites.

way (Table 3). The ensemble mean indicated that annual and monthly mean LST rate from site A to site B decreases, and then from site B to northern GC sites, the rate increases to its maximum at site G (~690,000 m^3/year, ~63000 m^3/month). The pattern of increasing LST rate along the coast is qualitatively consistent with previous studies (e.g., Splinter et al., 2011). The long-term annual LST rate at site G is about 10% more than the target rate used for calibration of LST models. The percentage of LST rate during non-modal conditions ($H_{s\text{-offshore}} > 1.7$ m) to total LST rate varies between 76% and 84% along the coast, acknowledging that GC can be classified as a storm-dominated coast. It should be noted that the estimations presented in Table 3 were obtained from an ensemble modeling which addresses the predefined sources of uncertainty (i.e., FD,WT, LSTM and their interactions). Addressing the residual uncertainties (the ones not addressed in this study, see the next section regarding the limitations of this work) would help increase the certainty of the estimations presented here.

Although the preliminary implication of this study is to consider some of the main sources of uncertainty for hindcasting wave-driven sediment transport patterns, this research has important implications for the study of climate change impacts on coastal sediment transport as well. For instance, given different offshore wave forcing datasets (probably obtained from wave simulations forced with global circulation models output) and coarse resolution of the forcing datasets (normally like the resolution used in this study or coarser), uncertainty arising from the inclusion/exclusion of local wind, different responses of LST models to new forcing conditions, it could be very challenging to provide reliable projections for the future patterns of wave-driven sediment transport.

5. Limitations and the way forward

This paper aimed to rank the uncertainty of the three predefined sources; the hindcast datasets (as the forcing of modeling framework) were used without any bias correction. Although the bias correction issue was not addressed, each member of the ensemble was weighted according to its skill to reproduce the reference LST data. This way the accuracy of forcing datasets was also considered implicitly (not explicitly). Applying one (or more) bias correction method (e.g., Lemos et al., 2020) to the forcing datasets to narrow uncertainty (arising from the choice of forcing datasets) is a part of future works.

Following Splinter et al. (2012), BMT WBM (2013), Sedigh et al. (2016), Vieira Da Silva et al. (2018), and Shaeri et al. (2019) the shape of the spectrum at the open boundary of the wave model was reconstructed using a JONSWAP spectrum (with a peak enhancement factor/Gamma of 3.3) for frequency distribution and Cos^n spectrum for directional distribution of wave energy. However, working with different types of spectrums- as a source of uncertainty- to reconstruct the wave energy at the wave model boundary and its impact on wave transformation as well as LST estimates requires more investigations. Moreover, integral parameters of total wave energy (H_s, T_p, D_m) were used to reconstruct the shape of spectrum for the boundary condition of wave model. This issue implies that a single peak spectrum was used. Although it was found that the aforementioned assumption is relatively reasonable (particularly for stormy conditions), having multi-modal spectrum rather than single peak spectrum still can be a source of uncertainty. More effort is required to develop reliable methods that can reproduce the shape of spectrum by knowing the integral parameters obtained from different partitions of wave energy (i.e., sea and swell). Additionally, the wave model was run under stationary mode to calculate the nearshore wave forcing samples (the MDA samples), and then the nearshore wave samples were introduced to RBF to reconstruct the whole time series of nearshore waves. This means that the energy field at each time step does not have any relation to the previous time steps and so, no time lag between sea states (wave energy conditions) of offshore and nearshore regions, is considered. Currently in the literature, there is a lack of a method that could reconstruct the whole times series of nearshore waves in a non-stationary mode with reasonable computational costs.

Apart from the uncertainty associated with wave forcing, wind forcing uncertainty also needs more investigations. Wind field obtained from the nearest sea-located grids of ERA5 and CAWCR datasets to GC, were extracted and averaged. The averaged wind forcing for each time step was applied uniformely to the computational domain. For wave transformation in local studies, this assumption can be made as the wind field usually might not vary significantly within small compactional domains (e.g., Ly and Hoan, 2018). Another issue is that the study area might have been influenced by the land/sea breeze effect extending an uncertain distance offshore. Due to the coarse resolution of CAWCR and EAR5, such an effect on wind forcing datasets (used in this study), probably could not be identified properly. Having a varying 2D wind field in the computational domain, waves at open boundary, and training a complex transfer function requires more investigations and could be the way forward. Additionally, in spectral wave models, wind sea interaction (both energy gain and dissipation) is estimated through formulation/parametrization. Hence, using different wave models using different formulations (e.g., Mike 21 vs SWAN) can yield different patterns of nearshore waves (e.g., Hoque et al., 2017). Understanding the relative importance of the parametrization to get a wider range of wave transformation uncertainty, could be another step of the current research.

Although for each site along the coast, an equilibrium barred profile was fitted with available hydrographic surveys, still, lack of high-quality data (the ones collected for a long-term period on a regular basis like monthly/seasonally) was prohibitive of assigning an equilibrium barred profile for each month/season. Addressing uncertainty arising from the

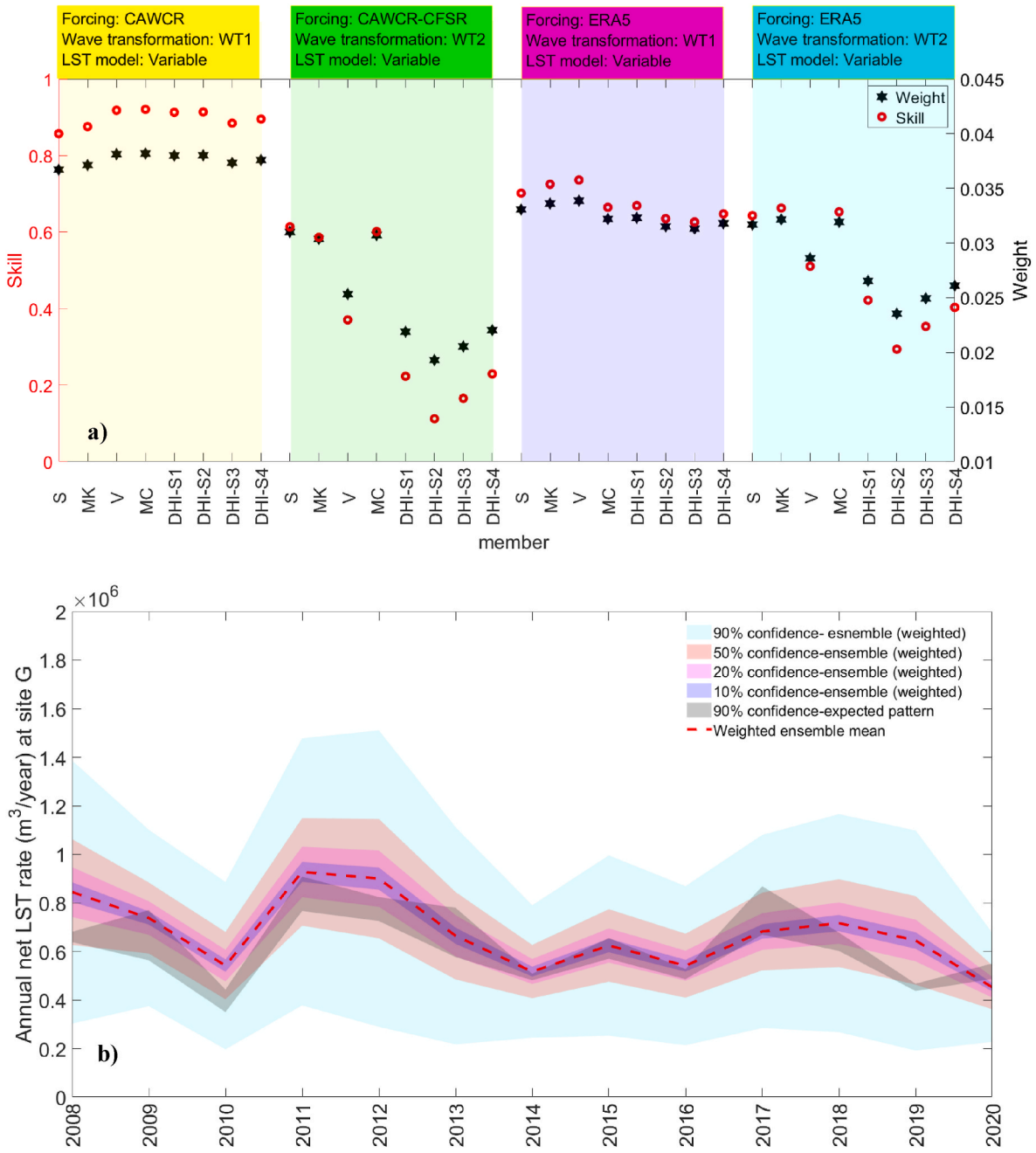

Fig. 13. a) Skill and weight of each ensemble member; b) Comparison of the annual net LST rate presented by the ensemble modelling with the reference LST data at site G; the expected pattern was obtained from the response of the calibrated LST models to GCB forcing (Gold Coast Buoy data) and used as the reference LST data.

Table 3
LST patterns obtained from the weighted ensemble mean.

Site	A	B	C	D	E	F	G
Inter-annul variability	0.31	0.31	0.27	0.25	0.24	0.24	0.24
Intra-annul variability	0.71	0.68	0.61	0.56	0.54	0.51	0.50
Long-term average net annual LST rate (m^3/year)	550,000	410,000	450,000	500,000	570,000	630,000	690,000
Long-term average net monthly LST rate (m^3/month)	46000	34000	38000	43000	49000	57000	63000
Net LST rate $_{\text{non-modal conditions}}$/Net LST$_{\text{all conditions}}$	84%	76%	78%	79%	80%	82%	84%

choice of bathymetry requires more investigations.

6. Summary and conclusion

In this paper, a simple ensemble modeling framework was employed to address a wide range of uncertainty in LST estimations at seven sites along the GC shoreline. Using different forcing datasets (CAWCR and ERA5), two wave transformation methods (WT1 and WT2), and eight LST models (four process-based models and four bulk formulae) led to the formation of an ensemble of 32 members by which uncertainty of

LST estimates was attributed to the main sources and their interactions. In the case of WT1, using ERA5 and CAWCR led to a more or less the same patterns of nearshore waves. But for the case WT2, it was found that the inclusion of local wind changed the patterns of wave attenuation (compared to the case WT1). As a result, for the case WT2, the patterens of alongshore energy flux was also impacted. Although for the case WT1, using one of the forcing datasets CAWCR/ERA5 and any of LST models led to more or less the same LST estimates, for the case WT2 by using the same forcing datasets and LST models, a significant range of uncertainty was observed. The process-based models (four set-ups of the DHI model) along with the model V were very sensitive to choice of wave transformation, compared to the rest of models. This issue implies that the interaction of wave transformation and LST models uncertainty are significant, and using a single LST model arbitrarily cannot provide a reliable estimate. Additionally, sites located on open coasts (sites D to G) are more vulnerable to uncertainty growth arising from the combination of WT and LST models. In general, for all sites (except site B), on the annual scale, ~50% of total uncertainty can be attributed to wave transformation uncertainty. Hence, in future works, much effort should be put into narrowing uncertainty associated with the wave transformation methods (here inclusion/exclusion of local wind). Uncertainty associated solely with the choice of LST models represents a 10–20% contribution to total uncertainty. The same goes for the choice of forcing datasets. But, the interaction of LST model and WT uncertainty is significant (>20% of total uncertainty), implying that in the case of using WT2, the choice of LST models plays another key role in the estimations. It seems that the relative importance of other non-linear interactions (e.g., FD-LSTM) on total uncertainty is negligible compared to the aforementioned uncertainty sources. It should be noted that the ranges of uncertainty for open coasts of GC (sites D to G) were much higher than those of semi-sheltered coasts (sites A, B, and C). The weighted ensemble mean was employed to investigate monthly and annual LST patterns along the coast, showing a decreasing trend in annual and monthly LST rates from site A to B, and an increasing trend from site B to G. The ranges of average monthly and annual LST rates vary from 410,000 m^3/year to 690,000 m^3/year, and from 34000 m^3/month to 63000 m^3/month, respectively. It should be pointed out that the presented estimates in this study were conditional to the predefined sources of uncertainty (i.e., FD, WT, LSTM and their interactions). Addressing the residual uncertainties (discussed in the previous section), in future works, would help increase the certainty of the estimations.

CRediT authorship contribution statement

Amin Reza Zarifsanayei: Conceptualization, Methodology, Software, Writing – original draft, Writing – review & editing. **José A.A. Antolínez:** Conceptualization, Methodology, Software, Writing – review & editing. **Amir Etemad-Shahidi:** Conceptualization, Methodology, Writing – review & editing, Funding acquisition, Supervision. **Nick Cartwright:** Conceptualization, Methodology, Writing – review & editing. **Darrell Strauss:** Conceptualization, Methodology, Writing – review & editing.

Declaration of competing interest

The authors declare that they have no known competing financial interests or personal relationships that could have appeared to influence the work reported in this paper.

Acknowledgment

The authors of this paper would like to thank Dr. Robert A. Holman for sharing the MATLAB codes of barred equilibrium beach profile and his fruitful comments on how to use them. The city of Gold Coast and the Queensland Government are much appreciated for providing the required data of this research, including bathymetries, hydrographic surveys, and wave buoys data. The authors would like to acknowledge the financial support from Griffith University. The first author was funded by GUPRS and GUIPRS scholarships. The authors also appreciate DHI for providing the license of the required models.

List of acronyms

Acronym	Explanation
BB	Brisbane wave Buoy
CAWCR	Center for Australian Weather and Climate Research
CSIRO	Commonwealth Scientific and Industrial Research Organisation
D_m	Mean Wave Direction (associated with total wave energy)
DSD	Directional Standard Deviation
DHI-S1	DHI-LITPACK setup#1
DHI-S2	DHI-LITPACK setup#2
DHI-S3	DHI-LITPACK setup#3
DHI-S4	DHI-LITPACK setup#4
EAR5	The fifth generation of ECMWF -European Centre for Medium-Range Weather Forecast- atmospheric reanalyses of the global climate
FD	Forcing Dataset
Gamma	Peak enhancement factor
GC	Gold Coast
GCB	Gold Coast wave Buoy
H_s	Significant Wave Height (associated with total wave energy)
KMA	K-mean Algorithm
LST	Longshore Sediment Transport
LSTM	Longshore Sediment Transport Model
MC	Modified CERC bulk formula
MDA	Maximum Dissimilarity Algorithm
MK	Modified Kamphuis bulk formula
PBB	Palm Beach wave Buoy
RBF	Radial Basis Function
S	Shaeri bulk formula
TOB	Tweed Offshore wave Buoy
T_p	Peak wave period (associated with total wave energy)
V	Van Rijn bulk formula
W_d	Wind Direction
W_s	Wind Speed

(*continued on next page*)

(*continued*)

Acronym	Explanation
WT	Wave Transformation
WT1	Wave Transformation #1: Wave conditions at offshore boundary without local wind effects
WT2	Wave Transformation #2: Wave conditions at offshore boundary plus local wind effects

Appendix A. Supplementary data

Supplementary data to this article can be found online at https://doi.org/10.1016/j.coastaleng.2022.104080.

References

Antolínez, J.A.A., Méndez, F.J., Camus, P., Vitousek, S., González, E.M., Ruggiero, P., Barnard, P., 2016. A multiscale climate emulator for long-term morphodynamics (MUSCLE-morpho). J. Geophys. Res. Ocean. 121, 775–791. https://doi.org/10.1002/2015JC011107.

Antolínez, J.A.A., Murray, A.B., Méndez, F.J., Moore, L.J., Farley, G., Wood, J., 2018. Downscaling changing coastlines in a changing climate: the hybrid approach. J. Geophys. Res. Earth Surf. 123, 229–251. https://doi.org/10.1002/2017JF004367.

Antolínez, J.A.A., Méndez, F.J., Anderson, D., Ruggiero, P., Kaminsky, G.M., 2019. Predicting climate-driven coastlines with a simple and efficient multiscale model. J. Geophys. Res. Earth Surf. 1596–1624. https://doi.org/10.1029/2018JF004790.

Belmonte Rivas, M., Stoffelen, A., 2019. Characterizing ERA-Interim and ERA5 surface wind biases using ASCAT. Ocean Sci. 15, 831–852. https://doi.org/10.5194/os-15-831-2019.

Benedet, L., Dobrochinski, J.P.F., Walstra, D.J.R., Klein, A.H.F., Ranasinghe, R., 2016. A morphological modeling study to compare different methods of wave climate schematization and evaluate strategies to reduce erosion losses from a beach nourishment project. Coast. Eng. 112, 69–86. https://doi.org/10.1016/j.coastaleng.2016.02.005.

Bishop-taylor, R., Nanson, R., Sagar, S., Lymburner, L., 2021. Mapping Australia ' s dynamic coastline at mean sea level using three decades of Landsat imagery. Remote Sens. Environ. 267, 112734.

BMT WBM, 2013. Coastal Process Modelling Suite.

Bonaldo, D., Benetazzo, A., Sclavo, M., Carniel, S., 2015. Modelling wave-driven sediment transport in a changing climate: a case study for northern Adriatic Sea (Italy). Reg. Environ. Change 15, 45–55. https://doi.org/10.1007/s10113-014-0619-7.

Bosshard, T., Carambia, M., Goergen, K., Kotlarski, S., Krahe, P., Zappa, M., Schär, C., 2013. Quantifying uncertainty sources in an ensemble of hydrological climate-impact projections. Water Resour. Res. 49, 1523–1536. https://doi.org/10.1029/2011WR011533.

Camus, P., Mendez, F.J., Medina, R., 2011a. A hybrid efficient method to downscale wave climate to coastal areas. Coast. Eng. 58, 851–862. https://doi.org/10.1016/j.coastaleng.2011.05.007.

Camus, P., Mendez, F.J., Medina, R., Cofiño, A.S., 2011b. Analysis of clustering and selection algorithms for the study of multivariate wave climate. Coast. Eng. 58, 453–462. https://doi.org/10.1016/j.coastaleng.2011.02.003.

City of Gold Coast, 2015. Gold Coast Surf Management Plan.

de Queiroz, B., Scheel, F., Caires, S., Walstra, D.J., Olij, D., Yoo, J., Reniers, A., de Boer, W., 2019. Performance evaluation of wave input reduction techniques for modeling inter-annual sandbar dynamics. J. Mar. Sci. Eng. 7 https://doi.org/10.3390/jmse7050148.

de Swart, R.L., Ribas, F., Calvete, D., Kroon, A., Orfila, A., 2020. Optimal estimations of directional wave conditions for nearshore field studies. Continent. Shelf Res. 196, 104071. https://doi.org/10.1016/j.csr.2020.104071.

DHI, 2017. Mike 21, Spectral Wave Module, Scientific Documentation.

DHL, 1992. Southern Gold Coast Littoral Sand Supply. Technical Report H85. Delft Hydraulics Laboratory.

Doering, J.C., Bowen, A.J., 1995. Parametrization of orbital velocity asymmetries of shoaling and breaking waves using bispectral analysis. Coast. Eng. 26, 15–33. https://doi.org/10.1016/0378-3839(95)00007-X.

Durrant, T., Greenslade, D., Hemar, M., Trenham, C., 2014. A Global Hindcast Focussed on the Central and South Pacific, CAWCR Technical Report.

Engelund, F., Fredsøe, J., 1976. A sediment transport model for straight alluvial channels. Hydrol. Res. 7, 293–306. https://doi.org/10.2166/nh.1976.0019.

Faivre, G., Strauss, D., Ollier, D., Tomlinson, R., 2017. Morphological modelling for the Gold Coast using wave classification. In: Australian Coasts & Ports Conference. https://search.informit.org/doi/10.3316/informit.925703088838570.

GCCM, 2017. Seaway Evolution - Morphological Trends and Processes - GCWA SRMP-006.

Hallin, C., Larson, M., Hanson, H., 2019. Simulating beach and dune evolution at decadal to centennial scale under rising sea levels. PLoS One 14, 1–30. https://doi.org/10.1371/journal.pone.0215651.

Hasselmann, K., Hasselmann, S., Bauer, E., Janssen, P.A.E.M., Komen, G.J., Bertotti, L., Lionello, P., Guillaume, A., Cardone, V.C., Greenwood, J.A., Reistad, M., Zambresky, L., Ewing, J.A., 1988. The WAM model - a third generation ocean wave prediction model. J. PHYS. Ocean. 18, 1775–1810. https://doi.org/10.1175/1520-0485(1988)018<1775:twmtgo>2.0.co;2.

Hersbach, H., Bell, B., Berrisford, P., Hirahara, S., Horányi, A., Muñoz-Sabater, J., Nicolas, J., Peubey, C., Radu, R., Schepers, D., Simmons, A., Soci, C., Abdalla, S., Abellan, X., Balsamo, G., Bechtold, P., Biavati, G., Bidlot, J., Bonavita, M., De Chiara, G., Dahlgren, P., Dee, D., Diamantakis, M., Dragani, R., Flemming, J., Forbes, R., Fuentes, M., Geer, A., Haimberger, L., Healy, S., Hogan, R.J., Hólm, E., Janisková, M., Keeley, S., Laloyaux, P., Lopez, P., Lupu, C., Radnoti, G., de Rosnay, P., Rozum, I., Vamborg, F., Villaume, S., Thépaut, J.N., 2020. The ERA5 global reanalysis. Q. J. R. Meteorol. Soc. 146, 1999–2049. https://doi.org/10.1002/qj.3803.

Holman, R.A., Lalejini, D.M., Edwards, K., Veeramony, J., 2014. A parametric model for barred equilibrium beach profiles. Coast. Eng. 90, 85–94. https://doi.org/10.1016/j.coastaleng.2014.03.005.

Hoque, M.A., Perrie, W., Solomon, S.M., 2017. Evaluation of two spectral wave models for wave hindcasting in the Mackenzie Delta. Appl. Ocean Res. 62, 169–180. https://doi.org/10.1016/j.apor.2016.11.009.

Kamphuis, J.W., 2010. Introduction to Coastal Engineering and Management, Advanced Series on Ocean Engineering. WORLD SCIENTIFIC. https://doi.org/10.1142/7021.

Kroon, A., de Schipper, M.A., van Gelder, P.H.A.J.M., Aarninkhof, S.G.J., 2020. Ranking uncertainty: wave climate variability versus model uncertainty in probabilistic assessment of coastline change. Coast. Eng. 158, 103673. https://doi.org/10.1016/j.coastaleng.2020.103673.

Larson, M., Hoan, L.X., Hanson, H., 2010. Direct formula to compute wave height and angle at incipient breaking. J. Waterw. Port, Coast. Ocean Eng. 136, 119–122. https://doi.org/10.1061/(ASCE)WW.1943-5460.0000030.

Le Cozannet, G., Bulteau, T., Castelle, B., Ranasinghe, R., Wöppelmann, G., Rohmer, J., Bernon, N., Idier, D., Louisor, J., Salas-y-Mélia, D., 2019. Quantifying uncertainties of sandy shoreline change projections as sea level rises. Sci. Rep. 9, 42. https://doi.org/10.1038/s41598-018-37017-4.

Lemos, G., Menendez, M., Semedo, A., Camus, P., Hemer, M., Dobrynin, M., Miranda, P. M.A., 2020. On the need of bias correction methods for wave climate projections. Global Planet. Change 186, 103109. https://doi.org/10.1016/j.gloplacha.2019.103109.

Ly, N.T.H., Hoan, N.T., 2018. Determination of nearshore wave climate using a transformation matrix from offshore wave data. J. Coast Res. 81, 14. https://doi.org/10.2112/SI81-003.1.

Mangor, K., Drønen, N.K., Kærgaard, K.H., Kristensen, S.E., 2017. Shoreline Management Guidlines - DHI. DHI.

Marsooli, R., Lin, N., Emanuel, K., Feng, K., 2019. Climate change exacerbates hurricane flood hazards along US Atlantic and Gulf Coasts in spatially varying patterns. Nat. Commun. 10, 1–9. https://doi.org/10.1038/s41467-019-11755-z.

Masselink, G., Hughes, M.G., 2003. Introduction to Coastal Processes and Geomorphology. Routledge, London.

Mathews, R.J., Stutz, M.L., Smith, A.W.S., 1998. A field investigation study to determine the properties of windblown beach sand. J. Coast Res. 14, 444–450.

Mil-Homens, J., Ranasinghe, R., van Thiel de Vries, J.S.M., Stive, M.J.F., 2013. Re-evaluation and improvement of three commonly used bulk longshore sediment transport formulas. Coast. Eng. 75, 29–39. https://doi.org/10.1016/j.coastaleng.2013.01.004.

Morim, J., Hemer, M., Wang, X.L., Cartwright, N., Trenham, C., Semedo, A., Young, I., Bricheno, L., Camus, P., Casas-Prat, M., Erikson, L., Mentaschi, L., Mori, N., Shimura, T., Timmermans, B., Aarnes, O., Breivik, Ø., Behrens, A., Dobrynin, M., Menendez, M., Staneva, J., Wehner, M., Wolf, J., Kamranzad, B., Webb, A., Stopa, J., Andutta, F., 2019. Robustness and uncertainties in global multivariate wind-wave climate projections. Nat. Clim. Change 9, 711–718. https://doi.org/10.1038/s41558-019-0542-5.

Murray, A.B., Antolínez, J.A.A., 2019. Forecasting future coastline change: HOW to address limitations and opportunities?. In: Coastal Sediments 2019. WORLD SCIENTIFIC, pp. 1077–1085. https://doi.org/10.1142/9789811204487_0094.

Ostrowski, R., 2016. On uncertainties in determination of sediment transport rates in coastal regions. Arch. Hydroeng. Environ. Mech. 63, 265–280. https://doi.org/10.1515/heem-2016-0017.

Pérez, J., Méndez, F.J., Menéndez, M., Losada, I.J., 2014. ESTELA: a method for evaluating the source and travel time of the wave energy reaching a local area. Ocean Dynam. 64, 1181–1191. https://doi.org/10.1007/s10236-014-0740-7.

Ranji, Z., Zarifsanayei, A.R., Cartwright, N., Soltanpour, M., 2022. Climate change impacts on tropical cyclones of the Arabian Sea: Projections and uncertainty investigations. Int. J. Climatol. https://doi.org/10.1002/joc.7523.

Sedigh, M., Tomlinson, R., Cartwright, N., Etemad-Shahidi, A., 2016. Numerical modelling of the Gold Coast Seaway area hydrodynamics and littoral drift. Ocean Eng. 121, 47–61. https://doi.org/10.1016/j.oceaneng.2016.05.002.

Shaeri, S., Etemad-Shahidi, A., Strauss, D., Tomlinson, R., 2019. Accelerated numerical simulation to investigate morphology changes around small tidal inlets. Coast Eng. J. 61, 535–558. https://doi.org/10.1080/21664250.2019.1651562.

Shaeri, S., Etemad-Shahidi, A., Tomlinson, R., 2020. Revisiting longshore sediment transport formulas. J. Waterw. Port, coastal. Ocean Eng. 146, 04020009 https://doi.org/10.1061/(ASCE)WW.1943-5460.0000557.

Smith, G.A., Hemer, M., Greenslade, D., Trenham, C., Zieger, S., Durrant, T., 2020. Global wave hindcast with Australian and Pacific Island Focus: from past to present. Geosci. Data J. 1–10 https://doi.org/10.1002/gdj3.104.

Splinter, K.D., Golshani, A., Stuart, G., Tomlinson, R., 2011. Spatial and temporal variability OF longshore transport along gold coast, Australia. Coast. Eng. Proc. 1, 95. https://doi.org/10.9753/icce.v32.sediment.95.

Splinter, K.D., Davidson, M.A., Golshani, A., Tomlinson, R., 2012. Climate controls on longshore sediment transport. Continent. Shelf Res. 48, 146–156. https://doi.org/10.1016/j.csr.2012.07.018.

Strauss, D., Mirferendesk, H., Tomlinson, R., 2007. Comparison of two wave models for Gold Coast, Australia. J. Coast Res.

Toimil, A., Camus, P., Losada, I.J., Le Cozannet, G., Nicholls, R.J., Idier, D., Maspataud, A., 2020. Climate change-driven coastal erosion modelling in temperate sandy beaches: methods and uncertainty treatment. Earth Sci. Rev. 202, 103110. https://doi.org/10.1016/j.earscirev.2020.103110.

Tolman, H.L., 1991. A third-generation model for wind waves on slowly varying, unsteady, and inhomogeneous depths and currents. J. Phys. Oceanogr. 21, 782–797.

Tonnon, P.K., Huisman, B.J.A., Stam, G.N., van Rijn, L.C., 2018. Numerical modelling of erosion rates, life span and maintenance volumes of mega nourishments. Coast. Eng. 131, 51–69. https://doi.org/10.1016/j.coastaleng.2017.10.001.

van Rijn, L.C., 2014. A simple general expression for longshore transport of sand, gravel and shingle. Coast. Eng. 90, 23–39. https://doi.org/10.1016/j.coastaleng.2014.04.008.

Vieira Da Silva, G., Murray, T., Strauss, D., 2018. Longshore wave variability along non-straight coastlines. Estuar. Coast Shelf Sci. 212, 318–328. https://doi.org/10.1016/j.ecss.2018.07.022.

Willmott, C.J., 1981. On the validation of models. Phys. Geogr. 2, 184–194. https://doi.org/10.1080/02723646.1981.10642213.

Zarifsanayei, A.R., Etemad-Shahidi, A., Cartwright, N., Strauss, D., 2020. Long-term prediction of longshore sediment transport in the context of climate change. Coast. Eng. Proc. 15 https://doi.org/10.9753/icce.v36v.papers.15.

Zyserman, J.A., Fredsøe, J., 1994. Data analysis of bed concentration of suspended sediment. J. Hydraul. Eng. 120, 1021–1042. https://doi.org/10.1061/(asce)0733-9429(1994)120:9(1021).